Catalysis Today 160 (2011) 213–227

Contents lists available at ScienceDirect

Catalysis Today

journal homepage: www.elsevier.com/locate/cattod

Precursor-mediated dissociation of *n*-butane on a PdO(1 0 1) thin film

Jason F. Weaver*, Jose A. Hinojosa Jr., Can Hakanoglu, Abbin Antony, Jeffery M. Hawkins, Aravind Asthagiri

Department of Chemical Engineering, University of Florida, Gainesville, FL 32611, USA

ARTICLE INFO

Keywords:
Alkane
Palladium oxide
Adsorption
Oxidation
C–H bond cleavage
σ-Complex

ABSTRACT

We investigated the molecular adsorption and dissociation of *n*-butane on a PdO(1 0 1) thin film using temperature-programmed reaction spectroscopy (TPRS) experiments and density functional theory (DFT) calculations. At low coverage, *n*-butane adsorbs on PdO(1 0 1) in a molecular state that is more strongly bound than *n*-butane physisorbed on Pd(1 1 1). This molecularly adsorbed state of *n*-butane on PdO(1 0 1) corresponds to a σ-complex that forms on the rows of coordinatively unsaturated (cus) Pd atoms of the oxide surface. TPRS results show that a fraction of the *n*-butane layer undergoes C–H bond cleavage below ~215 K and that the resulting fragments are completely oxidized by the surface upon continued heating. The evolution of product yields with the *n*-butane coverage as well as site blocking experiments provide strong evidence that the *n*-butane σ-complex serves as the precursor to initial C–H bond cleavage of *n*-butane on PdO(1 0 1). DFT calculations confirm the formation of an *n*-butane σ-complex on PdO(1 0 1). In the preferred bonding geometry, the *n*-butane molecule aligns parallel to a cus-Pd row and adopts a so-called η^1(2H) configuration with two coordinate H–Pd bonds per molecule. Our DFT calculations also show that σ-complex formation weakens C–H bonds, causing bond elongation and vibrational mode softening. For methane, we predict that coordination with a cus-Pd atom lowers the barrier for C–H bond cleavage on PdO(1 0 1) by more than 100 kJ/mol. These results demonstrate that dative bonding between alkane molecules and cus-Pd atoms serves to electronically activate C–H bonds on PdO(1 0 1) and suggest that adsorbed σ-complexes play a general role as precursors in alkane activation on transition metal oxide surfaces.

1. Introduction

Alkane activation by transition metals has attracted significant interest due to the desire to more effectively utilize alkanes in power generation applications and to develop improved strategies for transforming alkanes to chemicals of greater value. Indeed, developing catalysts that can efficiently convert methane to higher alkanes or organic oxygenates could have a profound impact on the commercial utilization of natural gas. The adsorption of alkanes on solid surfaces has been investigated extensively, with most studies focusing on clean transition metal (TM) surfaces [1]. While this prior work has greatly advanced the fundamental understanding of alkane activation on metallic surfaces, there is a significant need to characterize the elementary interactions between alkanes and TM oxide surfaces as well. A key reason is that several applications of oxidation catalysis occur under conditions that cause TM surfaces to oxidize, often resulting in dramatic changes in catalytic properties.

Of particular relevance to the present study is the catalytic combustion of CH_4 in lean gas turbines. Prior studies show that Pd catalysts perform exceptionally well in this application because the catalysts oxidize to a PdO phase which has a high activity for methane oxidation [2–13]. These findings certainly provide strong motivation for investigating the surface chemistry of PdO in detail. In the present study, we investigated the adsorption and oxidation of *n*-butane on a PdO(1 0 1) thin film, focusing particularly on the role of adsorbed σ-complexes as precursors for initial C–H bond activation.

Previous investigations show that the initial dissociation of alkanes on transition metal surfaces can occur by two general mechanisms, namely, a direct mechanism and a precursor-mediated mechanism. In the direct mechanism, the alkane molecule dissociates in a single gas-surface collision without thermally accommodating to the surface. The probability for direct dissociation generally increases with increasing gas kinetic energy since energetic molecules can more readily surmount activation barriers for dissociation during a single collision. The precursor-mediated mechanism is fundamentally different from the direct

* Corresponding author at: Department of Chemical Engineering, University of Florida, P.O. Box 116005, Gainesville, FL 32611, USA. Tel.: +1 352 392 0869; fax: +1 352 392 9513.
E-mail address: weaver@che.ufl.edu (J.F. Weaver).

0920-5861/$ – see front matter © 2010 Elsevier B.V. All rights reserved.
doi:10.1016/j.cattod.2010.06.012

mechanism. In the precursor-mediated mechanism, alkanes first adsorb into a molecular state and then dissociate. In this process, the molecularly adsorbed species acts as a precursor to dissociation, and a kinetic competition between desorption and dissociation determines the net probability for dissociation. Since the molecular adsorption of alkanes is non-activated, precursor-mediated dissociation becomes increasingly more probable as the gas kinetic energy decreases and should thus be dominant under typical reaction conditions.

Key characteristics of alkane dissociation by the precursor-mediated mechanism are known from investigations with metal surfaces. Compared with a single gas-surface collision, adsorbing into the molecular state affords an alkane with a greater opportunity to explore the reactive potential energy surface and dissociate by a low energy pathway(s). However, since the alkane molecule dissipates its energy during adsorption, dissociation by the precursor-mediated mechanism requires the existence of low energy pathways for C–H bond cleavage. While the dissociative chemisorption of alkanes is typically activated with respect to the gas-phase zero, facile dissociation has been reported for a few metal surfaces, including the reconstructed Ir(1 1 0) [14–17] and Pt(1 1 0) [18] surfaces and also defect sites of Ir(1 1 1) [19] and Pt(1 1 1) [20]. Dissociation is termed as facile for these systems because the activation energies for dissociation are lower than those for desorption. A trend that emerges from these prior studies is that low-coordination sites on metallic Pt and Ir surfaces are more reactive than close-packed terraces toward the activation of molecularly adsorbed alkanes. This higher reactivity appears to be a consequence of lower energy barriers for C–H bond cleavage, rather than resulting from longer lifetimes of alkane molecules at the low-coordination sites. An interesting possibility is that alkane dissociation barriers are strongly dependent on the local coordinative environment on non-metallic surfaces as well. Establishing such a relationship could aid in advancing a more general understanding of the factors which facilitate alkane activation.

We have recently found that propane undergoes facile C–H bond cleavage on the PdO(1 0 1) surface with dissociation occurring below 200 K in UHV [21]. The initial C–H bond cleavage occurs by a precursor-mediated mechanism in which a strongly-bound molecular state serves as the precursor to dissociation. Using temperature-programmed desorption (TPD) and density functional theory (DFT) calculations, we have shown that small alkanes bind strongly on PdO(1 0 1) by forming σ-complexes on coordinatively unsaturated (cus) Pd atoms of the surface [22]. The bonding of the alkane σ-complexes is analogous to that in organometallic complexes [23–25] and involves both electron donation from and backdonation to the alkane molecule and Pd d-states. In addition to enhancing the alkane binding strengths on PdO(1 0 1), σ-complex formation also weakens the coordinated C–H bonds as evidenced by bond elongation and softening of vibrational modes [22]. Thus, the formation of strongly-bound alkane σ-complexes on PdO(1 0 1) appears to electronically activate C–H bonds in addition to prolonging the surface lifetimes of the molecular precursors. We have recently shown that H_2 also forms a σ-complex on PdO(1 0 1) that acts as precursor to dissociation [26]. Taken together, these results point toward a general role of adsorbed σ-complexes as precursors in the activation of saturated molecules on PdO(1 0 1) and possibly other late TM oxides. The ability of the cus-Pd sites of PdO(1 0 1) to activate alkane C–H bonds bears a striking similarity to the high reactivity of under-coordinated sites of metallic surfaces reported in early studies of alkane activation [1].

In this paper, we extend our investigations of alkane adsorption and activation on PdO(1 0 1) to *n*-butane and further explore the properties of adsorbed alkane σ-complexes and their role as precursors for C–H bond activation on PdO(1 0 1). Similar to the smaller alkanes, we find that *n*-butane forms a relatively strongly-bound σ-complex on PdO(1 0 1) and present evidence that this species serves as the precursor for initial C–H bond cleavage of *n*-butane on the oxide. Our DFT calculations reveal that coordination to cus-Pd atoms on PdO(1 0 1) electronically activates C–H bonds of adsorbed alkane σ-complexes, thereby lowering energy barriers for C–H bond cleavage.

2. Experimental details

Previous studies [27,28] provide details of the three-level UHV chamber utilized for the present experiments. The Pd(1 1 1) crystal employed in this study is a circular disk (8 mm × ∼1 mm) spot-welded to W wires and attached to a copper sample holder that is held in thermal contact with a liquid nitrogen cooled reservoir. A type K thermocouple spot-welded to the backside of the crystal allows sample temperature measurements. Resistive heating, controlled using a PID controller that varies the output of a programmable DC power supply, supports maintaining or linearly ramping the sample temperature from 81 to 1250 K. Initially, sample cleaning consisted of sputtering with 600 eV Ar^+ ions at a surface temperature of 900 K, followed by annealing at 1100 K for several minutes. Subsequent cleaning involved routinely exposing the sample held at 856 K to an atomic oxygen beam for several minutes, followed by flashing the sample to 923 K to desorb oxygen and carbon oxides. As discussed previously [29], we limited the sample temperature to 923 K to maintain oxygen saturation in the subsurface reservoir and thereby ensure reproducibility in preparing the PdO(1 0 1) thin films used in this study. We considered the Pd(1 1 1) sample to be clean when we could no longer detect contaminants with X-ray photoelectron spectroscopy (XPS), obtained sharp low energy electron diffraction (LEED) patterns consistent with the Pd(1 1 1) surface, and did not detect CO production during flash desorption after oxygen adsorption.

A two-stage differentially-pumped chamber attached to the UHV chamber houses the inductively coupled RF plasma source (Oxford Scientific Instruments) utilized to generate beams containing oxygen atoms for this study. We refer the reader to prior work for details of the beam system [27,28]. To produce a PdO(1 0 1) thin film, we expose a Pd(1 1 1) sample held at 500 K to an ∼12 ML dose of gaseous oxygen atoms supplied in a beam, where we define 1 ML as equal to the Pd(1 1 1) surface atom density of 1.53×10^{15} cm^{-2}. This procedure generates a high-quality PdO(1 0 1) film that has a stoichiometric surface termination, contains ∼3.0 ML of oxygen atoms and is ∼12 Å thick [30,31]. The structure of the PdO(1 0 1) surface is discussed in detail below. We note that the Pd(1 1 1) sample is positioned ∼50 mm from the final collimating aperture and oriented at a 45° angle from the axis of the atomic oxygen beam during PdO film preparation. For these dosing conditions, we observe negligible gradients in the oxygen concentration across the oxidized Pd(1 1 1) sample, which suggests that the PdO films are uniformly thick across the substrate. For example, we find that the (1 0 1) LEED pattern persists as the incident electron beam is moved across the sample and observe only an abrupt disappearance of the LEED pattern as the electron beam passes the edge of the sample. We also observe negligible differences in TPRS data obtained after adsorbing molecules on PdO films grown at 45° versus highly glancing angles (>60°) relative to the atomic oxygen beam [26].

We delivered *n*-C_4H_{10} (Airgas 99.99%) to the sample surface using a calibrated beam doser with the sample located ∼50 mm from the end of the doser to ensure uniform impingement of the gases across the surface. Due to the large sample-doser separation, the direct flux was only ∼2.5 times higher than the background flux. After the *n*-butane exposures, we collected TPRS spectra by positioning the sample in front of a shielded mass spectrometer at a distance of ∼10 mm and then heating at a constant rate of

1 K s^{-1} until the sample temperature reached 923 K. Because the PdO film decomposes when heated to 923 K, it was necessary to prepare a fresh PdO thin film for each adsorption/reaction experiment. Although the total oxygen content varies slightly (<10%) among the PdO films studied, we find that TPRS results obtained from *n*-butane and other molecules are highly reproducible. To prepare well-developed, conformal PdO(1 0 1) films, we use an atomic oxygen exposure that brings the oxygen coverage well within the plateau region of the uptake curve [31]. As a result, small variations in the total oxygen content have a negligible effect on the surface structure and hence the chemical properties of the PdO films.

We estimate *n*-C_4H_{10} coverages by scaling integrated desorption spectra with TPD spectra obtained from a physically adsorbed monolayer of *n*-butane prepared on Pd(1 1 1) at 155 K and assuming a coverage of 0.14 ML for the *n*-butane layer on Pd(1 1 1). Prior studies using calibrated molecular beams show that a disordered monolayer of *n*-butane saturates on Pt(1 1 1) at a coverage of 0.14 ML [32,33] and that adsorption at ~150 K avoids the formation of more weakly-bound states at higher coverage. Given the similarities in *n*-butane TPD spectra between Pt(1 1 1) [32] and Pd(1 1 1) (*vide infra*), it is reasonable to assume that the *n*-butane monolayer saturates at the same coverage on both surfaces. To estimate atomic oxygen coverages, we scale O_2 TPD spectra with desorption spectra obtained from Pd(1 1 1) covered with 0.25 ML of atomic oxygen prepared by exposing the surface to O_2 at 300 K [29]. A fraction of the *n*-butane layer reacts with the PdO(1 0 1) surface during TPRS experiments to produce CO_2 and H_2O. In prior work, we calibrated CO_2 desorption yields by monitoring the production of CO_2 during CO oxidation on oxygen-covered Pd(1 1 1) and using a limiting amount of adsorbed atomic oxygen such that the CO_2 yield is equal to the initial atomic oxygen coverage. To estimate CO_2 yields in the present study, we assume that the ratio of CO_2 to O_2 scaling factors determined in previous work is applicable under the current experimental conditions. We have previously found that this assumption is reasonable.

3. Computational details

All the DFT calculations in this paper were performed using the Vienna *ab initio* simulation package (VASP) [34–37]. The calculation details for this study are similar to our earlier studies of the adsorption of H_2O, H_2, and alkanes on PdO(1 0 1) [22,26,38]. We use the projector augmented wave (PAW) [39,40] pseudopotentials provided in the VASP database. Calculations have been done using the Perdew–Burke–Ernzerhof (PBE) exchange-correlation functional [41]. An experimental band gap of ~1 eV has been reported for polycrystalline PdO [42], but standard GGA-DFT shows no band gap. We have previously tested the effect of using GGA+U to correct for the band gap, and while the adsorption energies are modified, the general conclusions about the relative stability of species on the surface are not affected. Furthermore, our earlier studies of adsorbed H_2O, H_2, and alkanes show better quantitative agreement between TPD-derived adsorption energies and barriers of elementary processes (e.g., dissociation and association of H_2O and H_2) using GGA-DFT values without the +U implementation. Since our primary interest is to determine the adsorption energies and surface reaction barriers, all calculations reported in this paper are done with standard GGA-DFT. A plane wave expansion with a cutoff of 400 eV was used, and the total energy calculations are done using the conjugate-gradient method for electronic relaxations, accelerated using Fermi-level smearing with a Gaussian width of 0.1 eV. In the initial search for relevant minima for the alkanes, the positions of the atoms are relaxed until the forces on all unconstrained atoms are less than 0.03 eV/Å, but we have further refined the most stable minima with a force criterion of 0.01 eV/Å. This stricter criterion is important for accurately evaluating the very low frequency modes (~50 cm^{-1}) of the alkanes on the surface. These modes mainly involve rotation of the molecule around the cus-Pd site, and without proper accuracy of the forces, these low frequency modes can appear as imaginary modes because of the flat potential energy surface at the cus-Pd site. The stricter force criterion changes the adsorption energy of the alkanes by ~1 kJ/mol. We identified several minima with η^1(H,H) interactions with cus-Pd atoms that lie within this range, and though there is some crossover in the favored configurations after relaxing the positions of the atoms to forces of less than 0.01 eV/Å, these changes are minor and do not affect the conclusions of this paper. The only minimum that shows a more noticeable difference in the nature of the bonding is the favored η^2 propane configuration which will be discussed in more detail later. In considering the adsorption energies reported in this paper, it is important to note that the DFT calculations do not capture the dispersion interactions. Dispersion can be included in the future [43,44] and may help to resolve differences between configurations with similar adsorption energies.

The structure of the PdO(1 0 1) film is modeled in the same manner as our earlier work. We represent the PdO(1 0 1) film with four layers (see Fig. 1), which corresponds to a thickness of ~9 Å. The bottom layer is fixed, but all other atoms in the oxide film and the adsorbates are allowed to relax. We use a vacuum spacing of 20 Å, which is sufficient to minimize any spurious periodic interactions in the surface normal direction. The PdO(1 0 1) film is obtained from the relaxed PdO bulk structure (a = 3.103 Å, c = 5.440 Å), but the film is strained (a = 3.057 Å, b = 6.352 Å) to match the reported experimental structure [30]. While experimentally the PdO(1 0 1) film is grown on the Pd(1 1 1) surface, the oxide film is sufficiently thick (~12 Å) that we assume the Pd(1 1 1) substrate may be ignored in our DFT calculations. Inclusion of the Pd(1 1 1) substrate would require large supercells due to the lattice mismatch between the oxide film and the Pd(1 1 1) surface. We use a 1×4 (2×2) surface supercell for alkanes adsorbed parallel (perpendicular) to the cus-Pd rows. Our choice of the lateral dimensions ensures that the adsorbed alkane has negligible intermolecular interactions with periodic images. A $4 \times 2 \times 1$ ($2 \times 4 \times 1$) **k**-point mesh was used for the 1×4 (2×2) surface supercell. We have performed tests to ensure that additional slab thickness and finer **k**-point meshes do not impact the results of the calculations.

We use the climbing nudged elastic band (NEB) method [45–47] to find minimum energy pathways (MEP) and identify transition states (TS) for C–H cleavage to methane on the PdO(1 0 1) surface. A normal mode analysis is performed on the TS to ensure that only one imaginary mode exists. The vibrational modes reported in this paper are obtained by fixing the substrate and allowing motion of only the alkane molecule. We use the finite difference method implemented within VASP to determine the Hessian and vibrational modes. Displacements of 0.02 Å are optimal to ensure that very low frequency modes (~50 cm^{-1}) found for alkanes adsorbed on the surface were accurately evaluated. We have performed tests of adsorbed methane that includes the motion of the cus-Pd atoms involved in the bonding and observe differences of only ~5 cm^{-1} in the vibrational frequencies. These differences are not sufficient to modify any of the conclusions reported in this paper.

4. Experimental results

4.1. Structure of the PdO(1 0 1) thin film on Pd(1 1 1)

Fig. 1 depicts the structure of the stoichiometric PdO(1 0 1) surface that we examined in this study. Bulk crystalline PdO has a tetragonal unit cell and consists of square planar units of Pd atoms fourfold-coordinated with oxygen atoms. The bulk-terminated

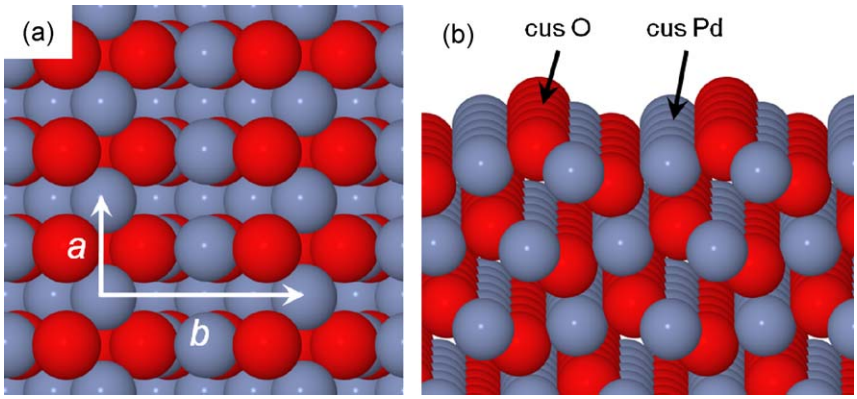

Fig. 1. (a) Top and (b) side view of the PdO($\bar{1}$ 0 1) thin film structure. The red and gray atoms represent O and Pd atoms, respectively. Rows of threefold-coordinated (cus) Pd and O atoms are indicated. The a and b directions correspond to the [0 1 0] and [1 0 1] crystallographic directions of PdO.

PdO(1 0 1) surface is defined by a rectangular unit cell of dimensions a = 3.04 Å and b = 6.14 Å, where the a and b lattice vectors coincide with the [0 1 0] and [$\bar{1}$ 0 1] directions of the PdO crystal, respectively. The PdO(1 0 1)–PdO surface consists of alternating rows of threefold- or fourfold-coordinated Pd or O atoms that run parallel to the a direction shown in Fig. 1. Thus, half of the surface O and Pd atoms are coordinatively unsaturated (cus) and likely to be more active than the fourfold-coordinated atoms for binding adsorbed molecules. The areal density of each type of coordinatively-distinct atom of the PdO(1 0 1) surface is equal to 35% of the atomic density of the Pd(1 1 1) surface. Hence, the coverage of cus-Pd atoms is equal to 0.35 ML (monolayer), and each PdO(1 0 1) layer contains 0.7 ML of Pd atoms and 0.7 ML of O atoms. Given that the film contains ~3.0 ML of oxygen atoms, we estimate that the PdO(1 0 1) film on Pd(1 1 1) consists of between four and five layers and has a total thickness of ~12 Å. In a prior study [30], we found that the PdO(1 0 1) structure aligns with the close-packed directions of the Pd(1 1 1) substrate and would expand by 0.46% and 3.4% in the a and b directions, respectively, to achieve commensurability with the metal substrate, which corresponds to unit cell dimensions of a = 3.06 Å and b = 6.35 Å.

4.2. TPRS of n-butane adsorbed on PdO(1 0 1) at 85 K

Fig. 2 shows representative TPRS spectra obtained after adsorbing n-butane on a PdO(1 0 1) film at 85 K. In this experiment, the first layer of n-butane is saturated, and the total n-butane coverage is initially 0.21 ML (60% of the cus-Pd site density). The n-butane TPD spectrum exhibits several features below ~250 K. Desorption from the n-butane multilayer produces the sharp peak at 117 K, while desorption from the first layer produces the features at higher temperatures. The region over which n-butane desorbs from the first layer exhibits two main features (α_2 and α_1) with maxima at ~138 and 218 K, which is qualitatively similar to the TPD spectra of smaller alkanes on PdO(1 0 1) [21,22]. However, as discussed in more detail below, the n-butane TPD spectra exhibit additional features that do not appear in TPD spectra of the smaller alkanes. The α_1 TPD peak is consistent with an n-butane σ-complex(es) that forms on the cus-Pd rows.

The evolution of CO_2 and H_2O during the TPRS experiments demonstrates that the PdO(1 0 1) surface is active for the complete oxidation of n-butane under the conditions examined. The behavior that we observe here is very similar to that of propane on PdO(1 0 1) [21]. A maximum CO_2 yield of 0.21 ML evolves during TPRS when the n-butane first layer is initially saturated and is equivalent to 0.60 C atoms per cus-Pd atom. Since the complete oxidation of one n-butane molecule consumes 13 oxygen atoms, we estimate that 0.68 ML of the surface oxygen atoms incorporate into the oxidation products, which is slightly less than the total O-atom density of 0.70 ML in the surface layer. As seen in Fig. 2, CO_2 desorbs predominantly in a single peak centered at 475 K, while the H_2O desorption trace exhibits a small peak at 337 K as well as a more intense feature at 475 K and a shoulder at 430 K. The small peaks at ~118 and 218 K seen in the 44 amu TPRS trace originate mainly from n-butane fragmentation in the ionizer, though a portion of the 218 K peak is consistent with CO_2 that adsorbed from the background or was produced by the oxidation of background CO. Based on prior investigations of H_2 and H_2O adsorption, we attribute the H_2O TPD peak at 337 K to desorption-limited water [26,38]. This feature accounts for about 14% of the H_2O that evolves. The higher temperature H_2O features must therefore arise from reaction-limited processes.

The concurrent desorption of H_2O and CO_2 at 475 K is characteristic of the reaction-limited oxidation of hydrocarbon fragments. The feature at ~430 K in the H_2O desorption trace also arises from a reaction-limited process, but an analogous feature is absent from the CO_2 trace. Water TPRS spectra obtained from H_2-exposed PdO(1 0 1) exhibit a reaction-limited feature near 430 K in addition to desorption-limited water [26]. This observation led us to conclude that the oxidation of H_2 on PdO(1 0 1) occurs by multiple pathways; a low energy pathway(s) produces H_2O below ~300 K,

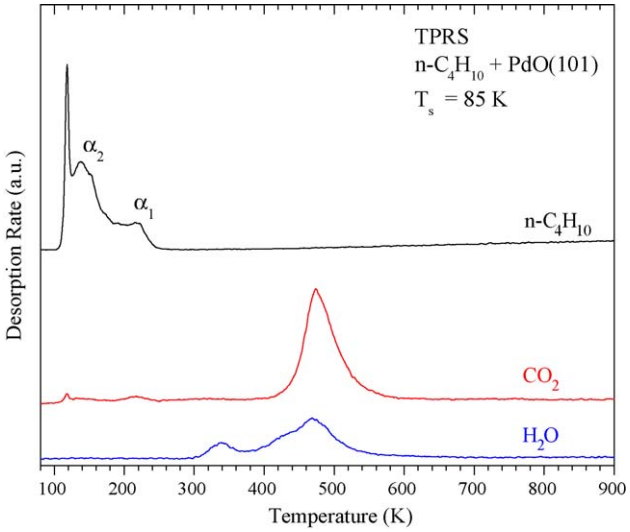

Fig. 2. TPRS spectra of n-butane (m/z = 29), CO_2 (m/z = 44), and H_2O (m/z = 18) obtained from a PdO(1 0 1) thin film after adsorbing ~0.21 ML of n-butane at 85 K. The traces show that CO_2 and H_2O evolve in a reaction-limited peak centered at ~475 K. A heating rate of 1 K s^{-1} was used in this experiment.

and a higher energy pathway(s) produces the reaction-limited H_2O. Thus, the oxidation of adsorbed hydrogen atoms may be responsible for the H_2O desorption features at both 337 and 430 K seen in TPRS spectra obtained from *n*-butane-exposed PdO(1 0 1) (Fig. 2).

We estimate that about 50% of the total H_2O desorbs in the reaction-limited feature at 475 K, which we associate with the oxidation of hydrocarbon fragments. If the remainder of the H_2O arises from the oxidation of adsorbed hydrogen atoms, then we would conclude that each *n*-butane molecule releases a maximum of five hydrogen atoms below the temperature at which the carbon backbone undergoes rapid oxidation. However, this estimate represents an upper bound for the extent of *n*-butane dehydrogenation prior to carbon oxidation since H_2 adsorption from the background can contribute to the peaks at 337 and 430 K. In fact, a relatively small quantity of background H_2 can have a significant effect on the relative yields of H_2O. For example, if ~0.11 ML of the total H_2O originates from background H_2 adsorption, then the reaction-limited feature at 475 K would account for 90% of the H_2O that originates from *n*-butane oxidation. This would mean that *n*-butane initially dissociates by single C–H bond cleavage and that the resulting butyl groups undergo negligible dehydrogenation before rapidly oxidizing near 475 K.

Overall, the TPRS results demonstrate that a fraction of the *n*-butane molecules exposed to PdO(1 0 1) undergo dissociative chemisorption and that the resulting fragments are completely oxidized by the surface above ~450 K during TPRS. As with propane [21], we are unable to detect partial oxidation products and thus conclude that the complete oxidation of *n*-butane is strongly favored on PdO(1 0 1). Considering prior studies of alkane adsorption [1], we expect that the initial activation of *n*-butane on PdO(1 0 1) occurs by cleavage of a single C–H bond. Partial dehydrogenation of the alkyl (or alkoxy) groups may also occur prior to the desorption of H_2O and CO_2. The present data shows that the dissociated *n*-butane releases no more than half, and probably much less (*vide infra*), of its hydrogen atoms prior to completely oxidizing. For the remainder of this paper, we focus on the mechanism for initial *n*-butane activation and present evidence that an adsorbed σ-complex acts as a necessary precursor to initial C–H bond cleavage of *n*-butane on PdO(1 0 1).

4.3. TPD of n-butane physisorbed on Pd(1 1 1)

Fig. 3a shows *n*-butane TPD spectra obtained after generating various coverages of *n*-butane on Pd(1 1 1) at 85 K. At low coverage, *n*-butane desorbs from Pd(1 1 1) in a single peak centered at 195 K. Distinct peaks at 115 and 137 K emerge after the *n*-butane coverage surpasses 0.07 ML, while the peak at 195 K continues to intensify. This behavior agrees well with a previous report of the growth of *n*-butane layers on Pt(1 1 1) [32]. In that study, *n*-butane molecules were found to physisorb into a disordered layer up to a coverage of 0.14 ML and adopt a flat-lying geometry that allows each CH_n group to reside within the attractive region of the molecule–surface potential.

Above 0.14 ML, the *n*-butane molecules arrange into ordered phases on Pt(1 1 1), denoted as the low coverage (LC) and high coverage (HC) phases, and simultaneously start to populate the multilayer. The LC phase consists of flat-lying molecules in an ordered arrangement that saturates at 0.20 ML [32,33]. *n*-Butane molecules in the HC phase tilt away from the surface to allow a higher packing density, resulting in a saturation coverage of 0.35 ML for this phase. Desorption from the ordered phases is responsible for the TPD peak at 137 K as well as the broad region of desorption leading to the main peak at 195 K. Desorption from the multilayer produces the sharp peak at 115 K. On Pt(1 1 1), the ordered phases and the multilayer populate concurrently as the *n*-butane coverage initially increases above 0.14 ML at low temperature [32].

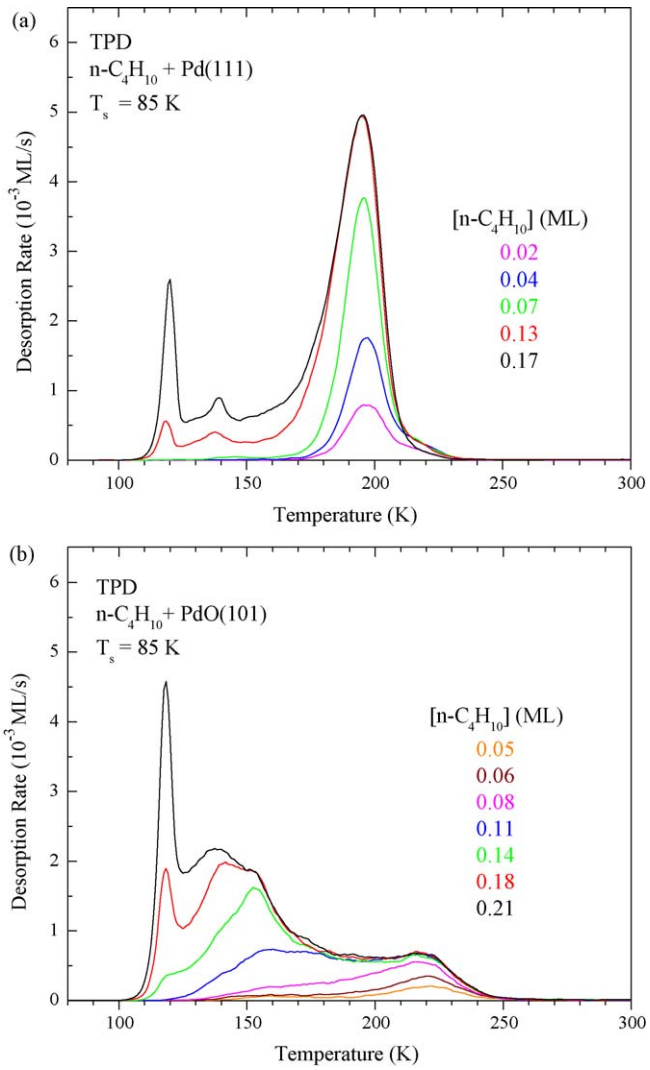

Fig. 3. TPD spectra of *n*-butane obtained after generating various *n*-butane coverages at 85 K on (a) Pd(1 1 1) and (b) PdO(1 0 1). The initial *n*-butane coverages are listed in each figure. For PdO(1 0 1), the total coverage is the sum of the total *n*-butane desorption yield plus the CO_2 desorption yield divided by four. A heating rate of 1 K s^{-1} was used in each experiment.

Similar behavior is evident in the *n*-butane TPD spectra obtained from Pd(1 1 1) in the present study (Fig. 3a). We note, however, that the more weakly-bound states begin to populate at 85 K before the disordered monolayer phase reaches its saturation coverage of 0.14 ML on Pd(1 1 1). This behavior demonstrates that the *n*-butane molecules are not mobile enough at 85 K to avoid the formation of metastable arrangements prior to saturating the disordered monolayer phase.

4.4. TPD of n-butane adsorbed on PdO(1 0 1)

Fig. 3b shows *n*-butane TPD spectra obtained after preparing various coverages of *n*-butane on a PdO(1 0 1) thin film at 85 K. Fig. 3b lists the total *n*-butane coverages, which are defined as the amount of *n*-butane that desorbs plus that which oxidizes to CO_2 and H_2O during the TPRS experiment. The *n*-butane TPD spectra are more complex than those obtained with smaller alkanes on PdO(1 0 1) [21,22]. As seen in Fig. 3b, *n*-butane initially desorbs in a broad peak (α_1) centered at 220 K that intensifies with increasing *n*-butane coverage above ~0.03 ML. Once the total coverage reaches 0.08 ML, the α_1 peak starts to saturate and more weakly-

bound states develop. Increasing the coverage to 0.08 ML causes a broad tail to emerge on the trailing edge of the α_1 peak, and distinct features at about 160 and 175 K become evident.

Further increasing the *n*-butane coverage causes desorption features to grow nearly sequentially at decreasing temperatures. The peak at 175 K effectively saturates when the total coverage reaches 0.11 ML, while the peak at 160 K continues to intensify and appears to shift to ~152 K as the coverage increases. A peak at ~137 K also develops above 0.11 ML and eventually becomes larger than the 150 K peak. The peak at 137 K resembles the feature that is associated with desorption from the LC and HC ordered phases on Pd(1 1 1). As mentioned in Section 2, various measurements show that the PdO(1 0 1) film uniformly covers the Pd(1 1 1) sample, so we are confident that the 137 K peak originates from *n*-butane desorbing from the oxide rather than metallic regions located at the perimeter of the sample. For both the oxide and the metal, the peak near 137 K develops only when the multilayer starts to form. The multilayer peak at 115 K first appears at a total coverage of 0.14 ML on PdO(1 0 1) and grows sharply as the coverage increases to 0.21 ML.

A comparison of the *n*-butane TPD spectra obtained from Pd(1 1 1) and PdO(1 0 1) provides insights into the nature of the *n*-butane adsorbed states on the oxide surface. Prior to multilayer formation, the TPD traces obtained from PdO(1 0 1) are very broad and exhibit several distinct peaks between ~130 and 250 K. In contrast, *n*-butane desorbs in only a single peak at comparable coverages on Pd(1 1 1). The TPD data thus shows that *n*-butane molecules adsorbed in the monolayer encounter a wider range of binding environments on PdO(1 0 1) compared with Pd(1 1 1). This diversity must be a consequence of the structural and compositional heterogeneity of the oxide surface. Despite this difference, the monolayer coverages on Pd(1 1 1) and PdO(1 0 1) appear to be similar. For example, *n*-butane TPD spectra obtained at a total coverage of ~0.18 ML exhibit multilayer peaks of nearly the same magnitude on both surfaces (Fig. 3). Integrating these traces above the multilayer peak, starting at 125 K, gives a coverage of ~0.14 ML for *n*-butane adsorbed in the monolayers on Pd(1 1 1) as well as PdO(1 0 1) for a total coverage of ~0.18 ML prepared at 85 K. This similarity may indicate that intermolecular interactions play a more important role than the molecule–surface interactions in determining the maximum coverages that are attained in the first layer.

The similar coverages also suggest that *n*-butane molecules adopt flat-lying configurations on PdO(1 0 1) at low coverage. An issue to consider further is the extent to which the LC and HC ordered phases develop on PdO(1 0 1). Compared with the dilute monolayer on Pd(1 1 1), *n*-butane molecules are more strongly bound in the α_1 state on PdO(1 0 1) and may offer greater resistance to ordering since the ordering is likely to disrupt their binding with the surface. On the other hand, nearly half of the first layer molecules on PdO(1 0 1) are more weakly bound than molecules in the α_1 state and may readily rearrange into ordered phases. Additional experiments are needed to examine these possibilities.

Another important difference between the TPD spectra obtained from the metal versus the oxide is that the α_1 peak appears at a higher temperature (220 K) than the TPD peak originating from *n*-butane physisorbed on Pd(1 1 1) at low coverage (195 K). We have reported similar behavior for methane, ethane, and propane [21,22], and have presented evidence that the α_1 states of these molecules correspond to alkane σ-complexes that form on cus-Pd sites of the PdO surface. The stronger binding of *n*-butane in the α_1 state on PdO(1 0 1) compared with *n*-butane physisorbed on Pd(1 1 1) is analogous to our previous findings with smaller alkanes and indeed supports the conclusion that the α_1 state of *n*-butane corresponds to an adsorbed σ-complex(es).

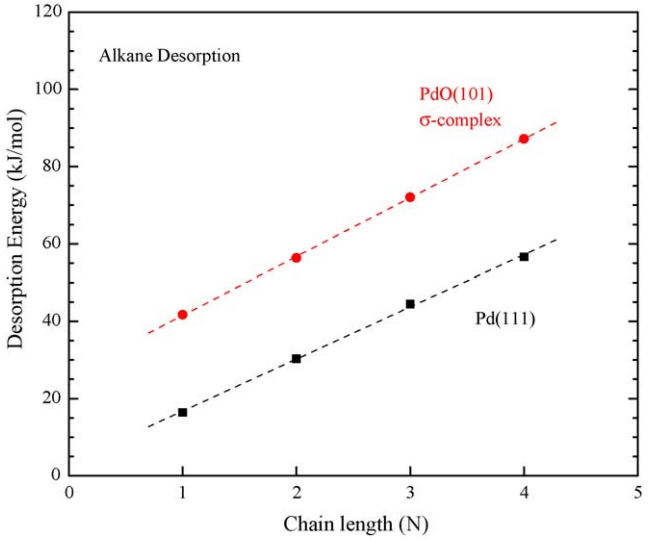

Fig. 4. Desorption (adsorption) energy versus chain length of linear C_1 to C_4 alkanes physically adsorbed on Pd(1 1 1) and adsorbed as σ-complexes on PdO(1 0 1). The desorption pre-factors for Pd(1 1 1) were taken from Ref. [48], and those for alkanes on PdO(1 0 1) represent maximum values determined from transition state theory [48].

4.5. Comparison of alkane binding energies on Pd(1 1 1) and PdO(1 0 1)

Analysis of the TPD data shows that the binding energy of the *n*-butane σ-complex closely follows the energy versus chain length (*E* versus *N*) trends that we reported recently for the σ-complexes of smaller alkanes on PdO(1 0 1) [22]. As seen in Fig. 4, the relationship between the binding energy and the chain length is well represented by a linear function for the C_1 to C_4 *n*-alkanes adsorbed on both Pd(1 1 1) and PdO(1 0 1). In a recent study [22], we attributed the non-zero intercept observed for C_1 to C_3 *n*-alkanes to a nearly constant contribution made by σ-complex formation on PdO(1 0 1). This interpretation implies that the molecule–surface dispersion interaction is the dominant cause of the linear increase in binding energy with increasing chain length of alkanes adsorbed on the oxide. This result is intriguing since one might expect that increasing the chain length would allow alkanes to form multiple dative bonds with the PdO surface and thereby experience a greater enhancement in binding on PdO(1 0 1) versus Pd(1 1 1) compared with smaller alkanes. While this possibility certainly exists, *n*-butane does not appear to be long enough to experience such additional enhancements in binding on PdO(1 0 1). The DFT results presented later support this interpretation.

We emphasize that the *E* versus *N* line shown in Fig. 4 represents an upper bound to the binding energies of alkanes adsorbed in the α_1 state on PdO(1 0 1). The reason is that we computed these binding energies using the Redhead equation and by taking maximum values of the desorption pre-factors appropriate for the α_1 peak temperatures. We estimated the desorption pre-factors using formulas derived from transition state theory for immobile alkane adsorbates as reported by Tait et al. [48]. As discussed in more detail in a previous report [22], the maximum desorption pre-factors appear to be more reasonable than the minimum values for describing the desorption of alkane σ-complexes from the PdO(1 0 1) surface. Using the Redhead equation, we estimate minimum and maximum values of 67.2 and 87.2 kJ/mol, respectively, for the *n*-butane σ-complex on PdO(1 0 1) and a binding energy of 56.6 kJ/mol for *n*-butane physisorbed on Pd(1 1 1). The TPD data thus suggest enhancements between about 10 and 30 kJ/mol for *n*-butane adsorbed on PdO(1 0 1) versus Pd(1 1 1). We expect that

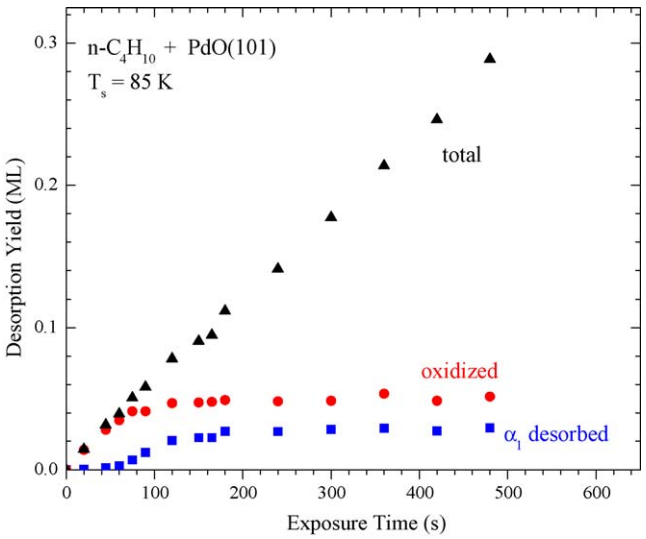

Fig. 5. Product yields obtained from PdO(1 0 1) as a function of the *n*-butane exposure time. The yields are estimated from TPRS traces obtained after *n*-butane adsorption on PdO(1 0 1) at 85 K. The plot shows the yield of *n*-butane that desorbs in the α_1 peak, the yield of *n*-butane that dissociates and subsequently oxidizes, and the total yield of *n*-butane, which is a sum of the desorption and dissociation yields.

the actual enhancement in binding is closer to the maximum value for reasons discussed above. Notably, the dative bond strengths that we estimate agree well with typical values (~20–60 kJ/mol) reported for mononuclear alkane σ-complexes [23].

4.6. Yields of desorbing versus oxidized n-butane

The evolution of product yields with the *n*-butane exposure provides evidence that the α_1 state serves as the precursor to the initial C–H bond cleavage of *n*-butane on PdO(1 0 1). Similar behavior observed in the dissociation of propane on PdO(1 0 1) [21] suggests a more general conclusion, namely, that the formation of adsorbed σ-complexes is a necessary first step in the activation of alkanes on the PdO(1 0 1) surface. Fig. 5 shows various product yields, as determined from TPRS data, as a function of the exposure time used to adsorb *n*-butane on PdO(1 0 1) at 85 K. The figure shows estimates of the yield of *n*-butane desorbing in the α_1 peak, the yield of *n*-butane that oxidizes, and the total *n*-butane yield. The total yield represents the total *n*-butane desorption yield plus the yield of *n*-butane that oxidizes, which is determined by dividing the CO_2 yield by four. We estimate the yield of *n*-butane desorbing in the α_1 peak by setting the lower limit of integration to 190 K in our analysis of the TPD traces.

Fig. 5 demonstrates that the oxidized yield and the α_1 desorbed yield evolve with the *n*-butane exposure in a similar manner, which implies a relationship between these products. Both yields increase initially with the *n*-butane exposure, but the rates of increase abruptly slow down at an exposure time of 120 s, and thereafter the oxidized and α_1 desorbed yields increase only marginally with exposure. In contrast, the total *n*-butane yield continues to increase rapidly with the *n*-butane exposure time well beyond 120 s. The correlation between the oxidized yield and the α_1 desorbed yield suggests that the α_1 state acts as a precursor to initial *n*-butane activation such that a fraction of the molecules adsorbed in the α_1 state undergo C–H bond cleavage rather than desorbing and are then oxidized completely by the surface at higher temperatures. A kinetic competition between desorption and dissociation of the precursor determines the fraction of molecules that dissociate by this mechanism.

The data gives maximum yields of ~0.03 and 0.05 ML for *n*-butane that desorbs in the α_1 peak and *n*-butane that oxidizes, respectively. Assuming that the *n*-butane which oxidizes originates from the α_1 state, we estimate a maximum coverage of 0.083 ML for *n*-butane molecules initially adsorbed in the α_1 state, which is equivalent to 0.94 C atoms per cus-Pd atom. Based on the geometric structures, an *n*-butane molecule aligned along a cus-Pd row would occupy no more than three Pd sites. Thus, at a coverage of ~0.08 ML, all of the *n*-butane σ-complexes could conceivably lie along the cus-Pd rows without experiencing strong crowding. However, we find that the dissociated fraction is a function of the coverage in the α_1 state. Initially, the dissociated fraction is about 95% of the total yield but decreases to 64% at saturation of the α_1 state. This behavior suggests that the *n*-butane dissociation probability depends on the coverage in the α_1 state, perhaps due to steric repulsion between neighboring molecules or butyl fragments at high coverage. While further study is needed to clarify this issue, intermolecular interactions could have different influences on *n*-butane adsorption versus dissociation on PdO(1 0 1).

4.7. Site blocking by $^{18}O_2$

To further characterize the nature of the *n*-butane σ-complex, we examined the influence of pre-adsorbed $^{18}O_2$ on the adsorption and dissociation of *n*-butane on the PdO(1 0 1) film. We have previously reported that O_2 chemisorbs molecularly on PdO(1 0 1) and dissociates to a negligible extent during TPD [49]. The molecularly chemisorbed O_2 saturates at a coverage of 0.28 ML (O-atom basis) at 85 K and desorbs in TPD peaks centered at 120 and 230 K. DFT calculations predict that O_2 binds on cus-Pd sites of the PdO(1 0 1) surface and could thus block the adsorption of *n*-butane onto these sites.

Fig. 6a and b show *n*-butane and CO_2 TPRS traces obtained after adsorbing ~0.30 ML of *n*-butane onto clean versus $^{18}O_2$ pre-saturated PdO(1 0 1) at 85 K. Fig. 6 also shows TPRS traces obtained in separate experiments that are discussed below. The TPRS data reveals that pre-adsorbing $^{18}O_2$ causes both the CO_2 and α_1 desorbed yields to decrease from the values obtained after adsorbing the same quantity of *n*-butane on clean PdO(1 0 1). Specifically, pre-saturating with $^{18}O_2$ causes the α_1 desorbed and CO_2 yields to decrease by ~35% and ~10%, respectively. This behavior provides additional evidence that the α_1 *n*-butane state acts as the precursor to initial C–H bond activation and that this state corresponds to *n*-butane molecules adsorbed on cus-Pd sites. The smaller decrease in the CO_2 yield compared with the α_1 desorbed yield indicates that the *n*-butane dissociation probability is higher on the $^{18}O_2$-covered surface than on clean PdO(1 0 1) for the conditions studied. Most likely, the apparent increase in the dissociation probability is a consequence of the lower *n*-butane coverage that is obtained on the $^{18}O_2$-covered surface. Finally, the *n*-butane peak near 137 K is more intense in the TPD spectrum obtained from the $^{18}O_2$ pre-covered surface relative to clean PdO(1 0 1). This difference reveals that the $^{18}O_2$ molecules do not completely block *n*-butane adsorption into the first layer but rather shift the population of *n*-butane states toward more weakly-bound configurations. A possibility is that the *n*-butane molecules continue to adsorb along the cus-Pd rows without accessing the α_1 state on the O_2-covered surface.

We have recently reported that the dissociation of H_2 on PdO(1 0 1) is also mediated by an adsorbed σ-complex and that blocking cus-Pd sites with O_2 suppresses H_2 dissociation [26]. However, pre-adsorbed O_2 is less effective at blocking cus-Pd sites for *n*-butane versus H_2 adsorption. For example, even though $^{18}O_2$ initially blocks about 80% of the cus-Pd sites, we estimate that the α_1 *n*-butane coverage reaches more than 65% of the α_1 saturation coverage (~0.05 versus 0.08 ML) obtained on an initially clean PdO(1 0 1) surface. In contrast, pre-saturating with O_2 causes the

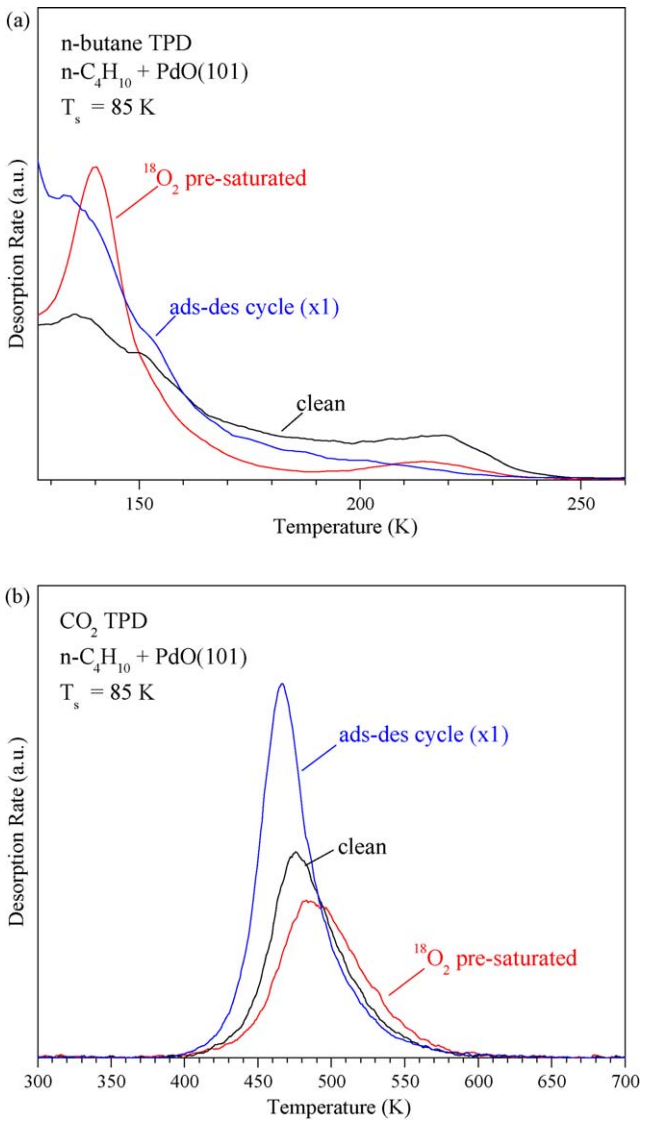

Fig. 6. TPRS traces of *n*-butane (top) and CO_2 (bottom) obtained after adsorbing *n*-butane at 85 K on clean PdO(1 0 1), $^{18}O_2$ pre-saturated PdO(1 0 1), and after one repeated adsorption–desorption cycle to generate butyl-covered PdO(1 0 1), as described in the text. The initial *n*-butane coverage is ~0.30 ML in the experiments with clean and $^{18}O_2$ pre-saturated PdO(1 0 1) and ~0.25 ML for the repeated adsorption–desorption experiment. The plot showing *n*-butane TPD traces omits the multilayer peak to accentuate the changes in the α_1 peak near 215 K. A heating rate of 1 K s^{-1} was used in each experiment.

H_2 dissociation yield to decrease to only 20% of its maximum value. The reason for this difference appears to be that *n*-butane molecules bind more strongly than H_2, and can thus displace O_2 from more weakly-bound states, and may also move to cus-Pd sites as $^{18}O_2$ desorbs during the TPRS experiment.

Support for this interpretation comes firstly from observations of $^{18}O_2$ desorbing as *n*-butane adsorbs onto $^{18}O_2$-covered PdO(1 0 1) at 85 K. Also, we find that the $^{18}O_2$ TPD yield is about 70% of the $^{18}O_2$ coverage prepared prior to *n*-butane adsorption (0.21 versus 0.29 ML) and that less than 0.01 ML of ^{18}O desorbs in other products, such as $H_2{}^{18}O$ and $C^{16}O^{18}O$. Notably, we do not observe organic oxygenates during TPRS from the mixed *n*-butane/$^{18}O_2$ layer. Rather, all of the dissociated *n*-butane appears to completely oxidize to carbon dioxide and water. Despite the partial displacement of $^{18}O_2$ that occurs, these measurements show that pre-adsorbed O_2 partially suppresses both the desorption of *n*-butane in the α_1 peak and the oxidation of *n*-butane to CO_2 and H_2O. As such, the results provide further support for concluding that the α_1 state corresponds to *n*-butane σ-complexes on cus-Pd sites and that the σ-complex is a necessary precursor to *n*-butane activation on PdO(1 0 1).

4.8. *n*-Butane adsorption–desorption cycles

We investigated the possibility of increasing the total *n*-butane dissociation yield on PdO(1 0 1) by repeating cycles of *n*-butane adsorption and desorption. In these experiments, we adsorbed ~0.25 ML of *n*-butane at 85 K and then heated to 270 K to completely evolve the desorbing fraction of the *n*-butane layer. We repeated this procedure multiple times before finally heating to 923 K and monitoring the desorption of products using TPRS. We limited the surface temperature to 270 K in an attempt to preserve the butyl groups produced in each heating step and also prevent surface reduction. Our rationale is that evolving the desorbing fraction should create vacant cus-Pd sites for additional *n*-butane adsorption and thus allow increasing the butyl coverage through a stepwise approach.

Fig. 6 shows *n*-butane and CO_2 TPRS traces obtained after conducting one adsorption–desorption cycle and then heating to 923 K after a second adsorption step at 85 K. The α_1 peak is very small in the *n*-butane TPD spectrum while the CO_2 peak is about 40% larger than that obtained after adsorbing *n*-butane on clean PdO(1 0 1). In fact, the increase in CO_2 yield after one cycle agrees quantitatively with the decrease in α_1 yield (~0.018 ML). This behavior demonstrates that *n*-butane molecules can adsorb onto the (nominally) butyl-covered surface and undergo C–H bond cleavage to generate higher butyl coverages than are attained in one adsorption step. We also collected TPRS spectra after performing up to three adsorption–desorption cycles to determine how the CO_2 and α_1 *n*-butane peaks evolve. The CO_2 yield changes marginally after the first cycle, and the α_1 peak further diminishes and is nearly absent after the third cycle. This trend suggests that *n*-butane molecules continue to adsorb in decreasingly smaller quantities after each step until reaching a saturation condition.

A simple model of the precursor-mediated activation of *n*-butane on PdO(1 0 1) can account for the changes in product yields that we observe after repeated adsorption–desorption cycles. In this model, a kinetic competition between desorption and dissociation of the adsorbed precursor determines the branching probability for dissociation, denoted as $S_o = k_r/(k_r + k_d)$, where k_r and k_d represent rate coefficients for dissociation ("reaction") and desorption, respectively. In the present analysis, we assume that *n*-butane dissociation occurs by single C–H bond cleavage to produce an adsorbed butyl group and a hydrogen atom. We further assume that only butyl groups remain on the cus-Pd rows. The dissociation probability is typically a strong function of the temperature and can also vary with adsorbate coverage. Using the precursor-mediated model, one may estimate the dissociation yield obtained during TPRS by integrating the butyl mole balance equation, but knowledge of the temperature dependence and possible coverage dependence of the dissociation probability is needed to perform the integration.

To simplify the analysis, we treat S_o as a constant and obtain an analytical equation that approximates the dissociation yield. Neglecting the temperature dependence of S_o can be reasonable if the desorption and dissociation of the *n*-butane precursor occur over a relatively narrow range of temperatures during TPRS. According to the model, the coverage of butyl groups produced by *n*-butane dissociation is given by $[R] = S_o[RH]_{max} + (1-S_o)[R]_o$, where $[R]_o$ and $[RH]_{max}$ represent the initial butyl coverage and the maximum coverage of *n*-butane in the α_1 state obtained on clean PdO(1 0 1), respectively. Within the context of this model, the dissociation probability S_o is equal to the dissociation yield, $[R]/[RH]_{max}$,

obtained after a single adsorption–desorption experiment and is estimated as $S_o = 0.64$ from the data shown in Fig. 5. Again, we emphasize that S_o in this model represents an effective dissociation probability that we apply to describe *n*-butane dissociation during TPRS.

The presence of butyl groups on the cus-Pd rows would lower the concentration of vacant cus-Pd sites available for *n*-butane adsorption. Assuming that *n*-butane molecules saturate these available sites, the *n*-butane coverage obtained on a surface initially covered with butyl groups at coverage [R] is given by $[RH] = [RH]_{max} - [R]$. This equation assumes that a butyl group and an *n*-butane molecule occupy the same number of surface sites. Applying these equations to repeated adsorption–desorption cycles gives the following equation for the butyl coverage generated after the *i*th *n*-butane exposure: $[R]_i = S_i[RH]_{max}$, where $S_i = \sum_{k=0}^{i} S_0(1 - S_0)^k$. Using $S_o = 0.64$, as estimated from the experimental data, the model predicts that $S_i = 0.88$, 0.96, and 0.98 for $i = 1$–3. These values differ by less than 3% from the total dissociation yields estimated from our experimental data.

The good agreement between the model and the experimental data suggests that the model captures essential features of the kinetics underlying *n*-butane activation on PdO(1 0 1). In the precursor-mediated model, a kinetic branching between desorption and dissociation determines the probability that a single *n*-butane molecule will dissociate. The present model assumes that this dissociation probability is independent of the *n*-butane coverage. We note, however, that our analysis uses the value of the dissociation probability determined for a saturated *n*-butane layer and that the yield data (Fig. 5) shows that the dissociation probability decreases from ~95% to 64% with increasing coverage in the α_1 state. We thus conclude that the coverage of adsorbed butyl groups and *n*-butane molecules have a similar effect on the *n*-butane dissociation probability when the combined coverage of these species is enough to saturate the cus-Pd sites. Indeed, the agreement between the predicted and the experimentally-determined yields supports the conclusion that butyl groups remain adsorbed on the cus-Pd rows under the conditions examined.

The increase in dissociation yield upon repeating adsorption–desorption cycles further suggests that butyl groups dehydrogenate to a limited extent during heating to 270 K. If the butyl groups did dehydrogenate, then the resulting H atoms would likely hinder the dissociation of *n*-butane molecules added to the surface in subsequent steps, in which case the CO_2 yield would not increase by the amount observed. Thus, the results also provide evidence that the butyl groups produced by *n*-butane activation remain stable up to at least 270 K. This stability could afford opportunities to steer the chemistry of alkyl groups on PdO(1 0 1) toward partial oxidation rather than complete oxidation to CO_2 and H_2O.

5. Computational results

5.1. Alkane σ-complexes

We used DFT to explore the bonding of *n*-butane σ-complexes on PdO(1 0 1) and to generally clarify how the nature of the alkane-Pd dative interaction influences C–H bond activation. In our earlier DFT study, we reported the formation of adsorbed σ-complexes for methane, ethane, and propane on PdO(1 0 1), where the alkanes coordinate with a cus-Pd atom(s) [22]. Charge density difference plots of methane adsorbed on cus-Pd atoms clearly show the donation–backdonation features, which are indicative of dative bonding. The adsorption energies from DFT, while not capturing the substantial dispersion interactions, show that alkane bonding on the PdO(1 0 1) surface is much stronger than corresponding adsorption on Pd(1 1 1). The C–H bonds involved in the coordinate interaction(s) are stretched from their gas-phase values. We also observe redshifts in vibrational modes associated with these bonds. These effects suggest that the dative bonding weakens the coordinated C–H bonds, making them easier to cleave. This model of alkane bonding on the PdO(1 0 1) surface can help to explain our experimental observations that the adsorbed σ-complexes of propane and *n*-butane serve as precursors to initial C–H bond cleavage.

In this paper, we extend our DFT results to the adsorption of *n*-butane on the PdO(1 0 1) surface. In our earlier study, we identified multiple η^1 and η^2 configurations for methane, ethane, and propane. In the present study, these minima were used as guesses to generate viable initial *n*-butane configurations that we subsequently relaxed. Fig. 7a and b shows the most stable η^1 and η^2 configurations of *n*-butane identified using DFT. *n*-Butane in the η^1(2H) configuration has two H atoms interacting with cus-Pd atoms on the surface and is favored over the single η^2(H,H) four-center bonding configuration by nearly 20 kJ/mol. We found a similar preference for η^1(2H) versus a single η^2(H,H) interaction for propane but with only a 3.3 kJ/mol difference [22]. This smaller difference between the η^1 and η^2 configurations of propane arises because the propane molecule can adopt an η^2(H,H) configuration involving the secondary carbon atom. We have also identified an η^2(C,H) configuration of propane (Fig. 8d) that is slightly favored by 1 kJ/mol over the η^2(H,H) configuration (not shown). In both of these configurations, the propane molecule avoids steric repulsion from the adjacent surface atoms and can thus adopt an optimal geometry for the η^2 interaction. A similar η^2 configuration is not possible for *n*-butane since it would bring non-bonded methyl groups too close to the PdO(1 0 1) surface. These steric interactions originate from the strong corrugation of the surface perpendicular to the cus-Pd row and occur when the long-chain alkanes align in that direction.

A clearer picture of the sensitivity of the four-center η^2(H,H) interaction to small geometric perturbations can be observed by comparing similar η^2 configurations for methane, ethane, propane, and *n*-butane. Fig. 8a–c shows the same η^2 configuration for methane, ethane, and propane as the one depicted for *n*-butane in Fig. 7b. The adsorption energies for these three configurations are 16.2, 21.9, and 13.9 kJ/mol, respectively. In methane and ethane, the η^2 configuration maintains the strong coordinate bond in addition to attractive non-bonded interactions between the methyl group and the cus-O atom, but the propane molecule experiences a sharp decrease in adsorption energy. This sharp decrease is maintained for the *n*-butane molecule, which has an adsorption energy of 12.3 kJ/mol. In summary, a comparison of the η^2 configurations involving the CH_3 group shows a sudden decrease in adsorption energy from ethane to propane. A visual inspection of Figs. 7a–c does not show much difference in the molecule–surface interaction of the methyl group, so the origin of the sudden decrease in adsorption energy is not obvious.

We initially examined the distortion cost of the molecule adsorbed on the surface. The distortion cost, or energy, can be obtained by evaluating the energy of the molecule in the adsorbed configuration with the surface removed and subtracting it from the energy of the gas-phase molecule. By this definition, a more negative value would indicate a greater strain or distortion energy, suggesting that intramolecular interactions are affected by adsorption on the surface. Our analysis shows that propane and *n*-butane have lower distortion energies than ethane, thus demonstrating that molecular strain due to the surface is not responsible for the unfavorability of the η^2 configuration for the longer-chain alkanes.

To separate the η^2 bonding interactions from other contributions from adjacent methyl groups, we took the adsorption configuration for propane shown in Fig. 7c and replaced the spectator methyl group with an H atom. The molecule and surface were then fixed, and only the new H atom was allowed to relax

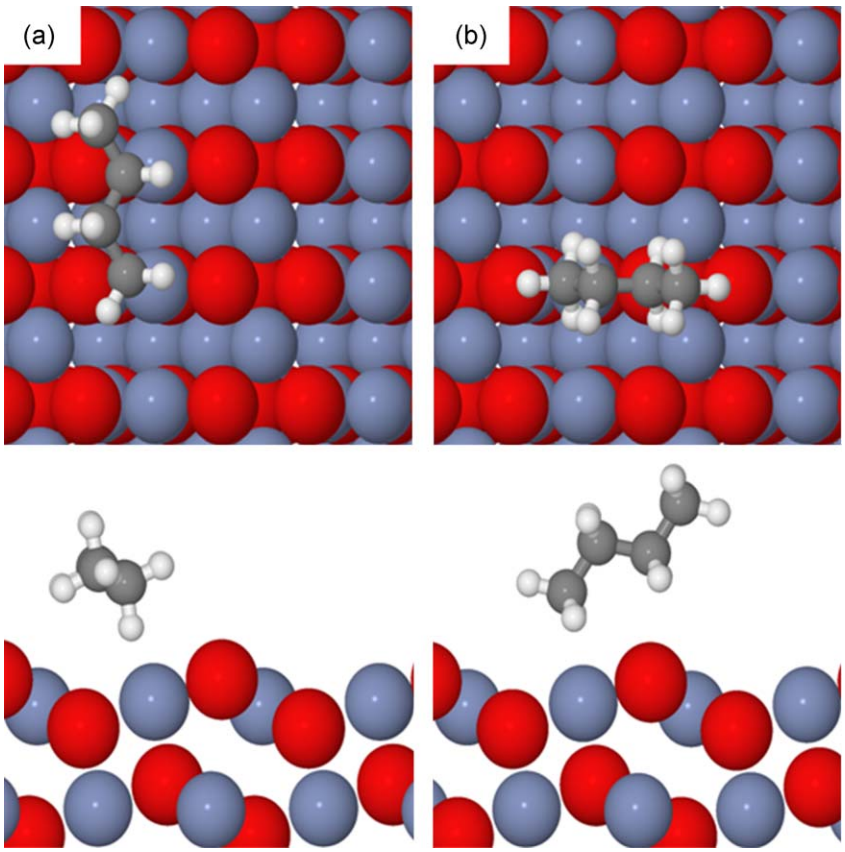

Fig. 7. The favored (a) η^1(2H) and (b) η^2(H,H) configurations identified for *n*-butane on the PdO(1 0 1) surface with E_{ads} = 31.2 and 12.3 kJ/mol, respectively. The η^1(2H) configuration involves two η^1 bonding interactions, while the η^2 configuration results in one weakened η^2 interaction.

to obtain an optimal C–H bond length. This procedure results in an ethane molecule bound to the surface in precisely the same manner as the propane molecule. The adsorption energy for this new ethane configuration is 13.4 kJ/mol, which is very similar to the propane and *n*-butane adsorption energies. Therefore, the spectator methyl groups of propane and *n*-butane are sufficiently repelled by the surface to prevent these molecules from achieving optimal bonding in the η^2 configuration. A more detailed analysis of the methyl group–cus-Pd interaction for ethane and the modified ethane shows that the modified ethane has a 12° rotation around the axis aligned along the cus-Pd rows. This rotation disrupts the sensitive four-center interaction of the η^2(H,H) configuration, resulting in a weaker bond. As noted earlier, this rotation is forced on the propane and *n*-butane configurations shown in Figs. 8c and 7b by the surface corrugation perpendicular to the cus-Pd row. For propane, this perturbed η^2 configuration can be avoided by moving the coordinate bond to the secondary carbon atom (see Fig. 8d), which allows the molecule to sit on top of a cus-Pd atom with the adjacent methyl groups pointing away from the surface. Such a configuration is not an option for *n*-butane since the additional methyl group would have to be oriented toward the surface. As noted above, we identified both η^2(H,H) and η^2(C,H) configurations for propane with very similar adsorption energies. These two configurations are related by a small rotation around the axis aligned normal to the cus-Pd rows, which is distinct from the unfavorable rotation around the axis aligned along the cus-Pd rows that disrupts the η^2 interaction for propane and *n*-butane in Figs. 7b and 8c. *n*-Butane cannot adopt either the η^2(H,H) or η^2(C,H) configuration through its CH_2 group because of the considerable steric interactions with the PdO(1 0 1) surface, which forces the weak bonding observed in Fig. 7b.

The above analysis clearly reveals that the methyl η^2 configuration is highly sensitive to the local geometry since the configuration involves a four-center interaction. This sensitivity prevents stable minima of η^2 configurations from forming along the cus-Pd rows. As seen in the η^2 configuration of methane (Fig. 8a), the downward-oriented H atoms lie in the direction of the cus-Pd rows. Rotating the methane molecule such that the downward-oriented H atoms lie perpendicular to the cus-Pd rows results in a relaxed η^1 configuration with only one H–Pd interaction. These results indicate that the η^2(H,H) bonding is also disrupted if the H atoms are brought close to the adjacent cus-O atoms, which leaves the configuration in Fig. 8a as the only stable η^2 configuration for CH_4. Clearly, longer-chain alkanes that lie along the cus-Pd row will also be unable to adopt such an η^2 configuration. To confirm this idea, we prepared initial η^2 configurations of ethane, propane, and *n*-butane lying parallel to the cus-Pd rows, and, as expected, each of these configurations relaxes into η^1 configurations such as that shown in Fig. 7a. With alkanes able to form only one η^2 bond, and such bonding being weaker for the larger alkanes, it is clear that the η^1 configurations along the cus-Pd rows will be the overwhelmingly favored adsorbed state of *n*-butane and longer straight-chain alkanes.

Propane holds a unique position in the transition from η^2 to η^1 configurations because it can adopt an η^2 configuration on its secondary carbon, which results in η^1 and η^2 configurations that are very similar in energy (~3 kJ/mol). For *n*-butane and larger straight-chain alkanes, DFT suggests that the component of the adsorption energy due to dative bonding interactions will scale as the number of η^1 interactions formed. For propane and *n*-butane, only two η^1 bonds can form due to the registry of these molecules on the PdO(1 0 1) surface. For propane, both of these bonds form on the CH_3 groups, while *n*-butane has one bond at a CH_3 group

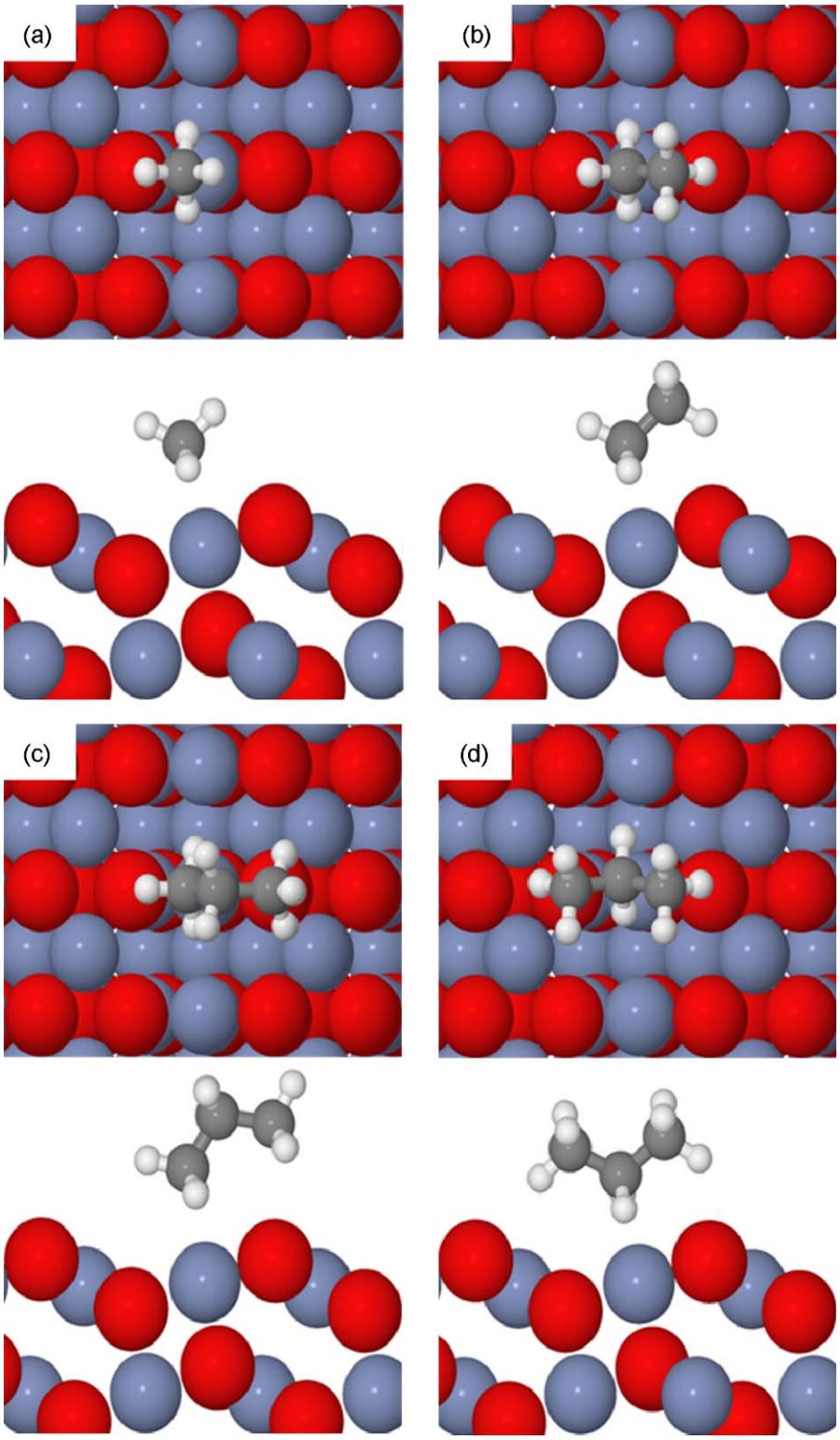

Fig. 8. The same η^2 configuration for (a) methane, (b) ethane, and (c) propane as the favored η^2 configuration identified for *n*-butane on the PdO(1 0 1) surface (see Fig. 7b). The adsorption energies for the terminal η^2 configurations of methane, ethane, propane, and *n*-butane are 16.6, 22.7, 13.9, and 12.3 kJ/mol, respectively. The favored η^2 configuration for propane involves η^2 bonding with the secondary carbon as shown in (d) with an adsorption energy of 25.7 kJ/mol.

and the other at a CH_2 group. The adsorption energies of propane and *n*-butane in the η^1(2H) configuration are 27.7 and 31.2 kJ/mol, respectively. While these values may indicate subtle differences in the strengths of η^1 bonds involving primary versus secondary C–H bonds, the energy difference is slight and could arise solely from non-bonding interactions. Future studies with longer alkanes that form three or more bonds will help to clarify this issue. Calculations that explicitly include the molecule–surface dispersion interaction are also required to fully account for the non-bonding interactions.

We examined the adsorption of *n*-pentane on the PdO(1 0 1) surface as well and find that the favored bonding geometry is the η^1(3H) configuration shown in Fig. 9. In this configuration, the

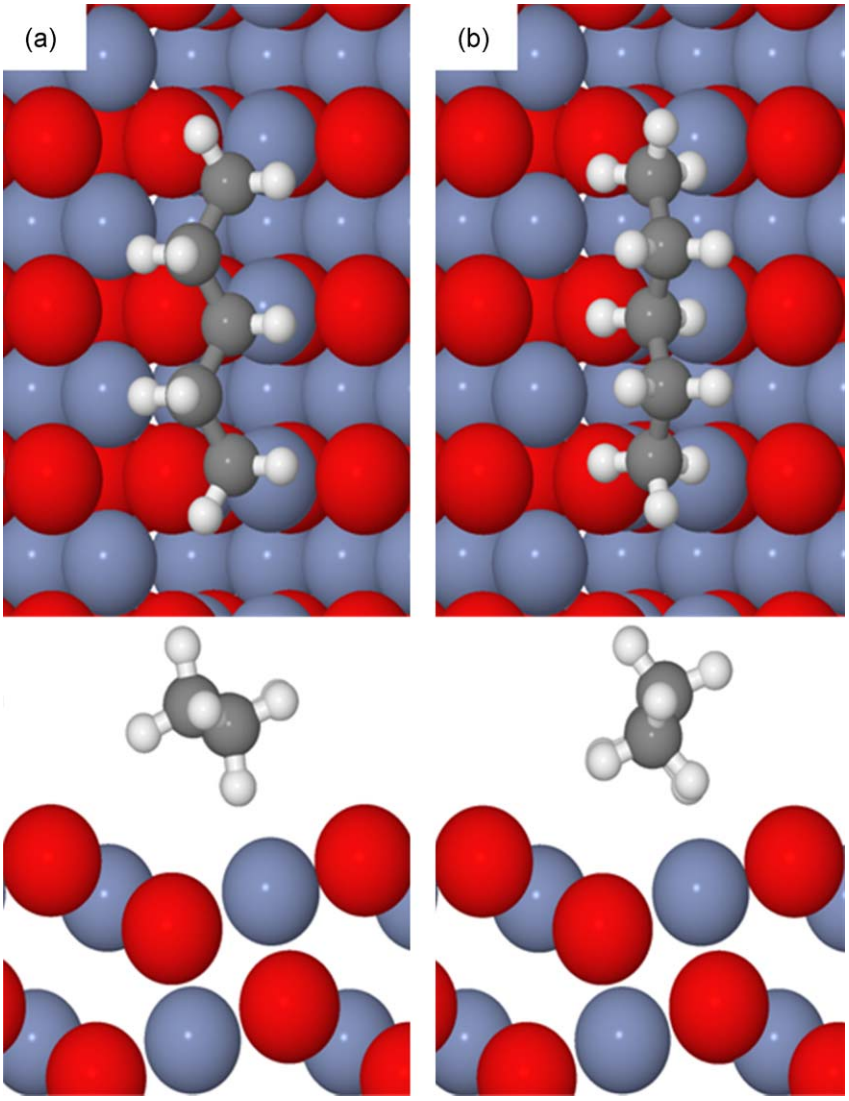

Fig. 9. The favored η^1(3H) configurations for *n*-pentane with three H–Pd interactions with adsorption energies of (a) 41.2 kJ/mol and (b) 40.7 kJ/mol.

n-pentane molecule forms three η^1 bonds, one at each primary carbon atom and one at the central CH_2 group. The adsorption energies of the η^1 configurations of *n*-pentane are ~40 kJ/mol. This value of the adsorption energy is close to 3/2 that of the η^1(2H) propane configuration, which matches the ratio of η^1 bonds. This result suggests that the constant offset found in the experimentally-determined *E* versus *N* relationship for methane to *n*-butane (Fig. 4) should break down and exhibit an abrupt increase at *n*-pentane if each of the η^1 bond strengths is in fact similar. Subsequent *n*-alkanes might also show a stepwise behavior in the offset, depending on the registry between the *n*-alkanes and the cus-Pd rows.

As shown in Fig. 9, n-pentane molecules adsorbed in the η^1 configuration have freedom to rotate toward the neighboring fourfold-coordinated Pd row while preserving the coordinate H–Pd bonds with the cus-Pd row. For example, the configurations shown in Fig. 9a and b are related by a rotation around an axis parallel to the cus-Pd rows. Both of these configurations share the same coordinate bonding, differing only in their non-bonding interactions with the surrounding atoms. The difference in the adsorption energy of these two configurations is 0.5 kJ/mol. While not shown, we have found similar results for *n*-butane and can conclude that the η^1 configurations have more rotational freedom since the two-center Pd–H interaction is not as restrictive as the four-center interaction of the η^2 configuration. The rotational freedom of the η^1 configurations may allow these alkane σ-complexes to maximize their dispersion interaction with the surface while maintaining relatively strong dative bonding with the cus-Pd row. In effect, the *n*-alkane σ-complexes could adopt a flat-lying geometry relative to the local facet and experience a linear increase in the strength of the dispersion interaction with increasing chain length. Thus, the experimentally-observed *E* versus *N* relation (Fig. 4) appears to be consistent with propane and *n*-butane adsorbing in the η^1 configuration. Additional work that accurately includes dispersion interactions will be needed to test this idea.

In our earlier study of alkane σ-complexes on PdO(1 0 1), we reported lengthening (~1.55%) of the two C–H bonds of CH_4 that coordinate with the cus-Pd atom. Furthermore, vibrational modes involving the symmetric and asymmetric C–H stretch of the weakened C–H bonds redshift from the corresponding gas-phase values by ~200 cm^{-1}. The magnitude of these redshifts is much larger than those observed for alkanes on metal surfaces [1,50] and can be attributed to the dative bonding interaction on PdO(1 0 1). Table 1 shows the C–H bond stretching and mode softening of the symmetric and asymmetric stretch frequencies for the relevant minima identified for the alkanes on PdO(1 0 1) along with the relevant H–Pd bond distances for atoms involved in the coordinate bonding.

Table 1
The C–H and Pd–H bond lengths, along with the associated mode softening of the C–H stretch frequencies, for the relevant minima of alkanes from methane to *n*-butane. Similar values for *n*-pentane, except for the mode softening, are also included. The percent stretch of each C–H bond length with respect to the gas-phase value is provided in brackets. The primary (CH_3) and secondary (CH_2) groups on the alkane are distinguished.

Configuration	C–H stretch (Å) [%]		Pd–H (Å)		Mode softening (cm^{-1})
	CH_3	CH_2	CH_3	CH_2	
η^2 methane	1.114 [1.55]	–	2.160	–	208, 169
η^2 ethane	1.118, 1.123 [1.64, 2.09]	–	2.186, 2.126	–	232, 222
η^2 propane	–	1.106, 1.146 [0.27, 3.89]	–	2.601, 1.937	470
η^1 propane	1.128 [2.23]	–	2.008	–	284, 262
η^1 *n*-butane	1.127 [2.36]	1.138 [3.08]	2.030	1.974	362, 264
η^1 pentane	1.125, 1.122 [2.36, 1.99]	1.138 [2.89]	2.017, 2.152	2.012	–

Methane also shows softening of a bending mode (not shown), but for the other alkanes the dramatic softening (>50 cm^{-1}) is restricted to stretching frequencies dominated exclusively by the C–H bonds interacting with the cus-Pd atoms. The values for methane, ethane, and propane are slightly different than the values reported in our earlier study [22] because we have used a force criterion of 0.01 (0.03) eV/Å and atomic displacements for the normal mode calculations of 0.02 (0.05) Å in the present (earlier [22]) study. We found these changes to be necessary to properly refine the low frequency modes involved in rotation of the molecule on the surface. The change in the values reported in Table 1 are all minor and do not affect the conclusions from our earlier study, except for the identification of a new η^2(C,H) propane configuration. As noted above, this configuration is very close in energy to the η^2(H,H) propane configuration reported in our earlier study [22]. The inclusion of dispersion may differentiate these two configurations, but with our current DFT values, we can expect both to be present and indistinguishable by TPD.

We predict small increases in the percentage of C–H bond stretching with increasing alkane chain length independent of the type of bonding (η^1 versus η^2). Since hyperconjugation can stabilize the weakening of a C–H bond, an ethane σ-complex may experience slightly more elongation of the C–H bonds and shorter H–Pd bonds compared with methane. The DFT results confirm this expectation (Table 1). Also, the mode softening scales with the extent of C–H bond stretching and therefore is more pronounced for longer alkanes. The alkane chain length dependence of C–H bond stretching should become negligible with larger alkanes, and in fact, we see very little difference in the C–H bond lengths between *n*-butane and *n*-pentane. Because of the lack of symmetry between the two downward-oriented C–H bonds within the η^2(C,H) propane configuration, the mode softening is associated with only one of the C–H bonds and is quite large at 470 cm^{-1}. This magnitude of mode softening is the largest we have found among all of the alkane configurations and suggests that η^2(C,H) and η^2(H,H) configurations can be distinguished with vibrational spectroscopy. Furthermore, the dramatic difference in mode softening between the two configurations may also result in differences in C–H bond cleavage, but future studies of the C–H bond scission will be needed to confirm this hypothesis.

A pronounced effect is also observed in the η^1 configuration of *n*-butane where the mode softening associated with the CH_2 group is greater by nearly 100 cm^{-1} over that associated with the CH_3 group. The percent change in the C–H bond lengths also reflects the difference in mode softening as the primary (secondary) C–H bond stretches by 2.36 (3.08)% from the corresponding gas-phase values. The difference between primary and secondary C–H bonds does not seem to be entirely attributable to differences in H–Pd interactions since those bond lengths differ only by ~0.05 Å. In general, the secondary C–H bonds are more easily cleaved than the primary bonds due to hyperconjugation (i.e., resonance stabilization), and we believe that this effect is responsible for the greater mode softening of the secondary C–H bonds that we predict. Therefore, the DFT calculations suggest that cleavage of the secondary C–H bonds of *n*-butane will be more facile than the primary C–H bonds. Such a hypothesis based on mode softening and bond stretching will have to be confirmed with future studies of C–H activation barriers for the alkanes.

5.2. Dissociation pathways for η^2 methane

Understanding the mechanisms and barriers for C–H bond cleavage of alkanes in different bonding configurations (η^1 versus η^2, primary versus secondary) will provide important insights for understanding the factors which influence alkane activation on the PdO(1 0 1) surface. This information can be subsequently used to explore modifications of the surface to enhance activity for alkane oxidation. Nevertheless, fully exploring all of the possible reaction pathways for methane to *n*-butane is beyond the scope of this paper. Instead, we present results for C–H activation of the η^2 methane configuration shown in Fig. 8a. The adsorbed CH_4 molecule has two types of C–H bonds that are candidates for cleavage. The first is the non-interacting, upward-oriented C–H bond pointed toward the cus-O atom, and the second is one of the two equivalent C–H bonds involved in the η^2 interaction with the cus-Pd atom. We have not considered the other upward-oriented C–H bond since our recent DFT study of H_2 on PdO(1 0 1) indicates that the preferred binding site for an H atom is on top of a cus-O atom [26]. Therefore, the first pathway we investigated is a simple transfer of the upward-oriented H atom to the adjacent cus-O site as shown in Fig. 10a. This pathway yields a large C–H bond activation barrier of 167 kJ/mol, which suggests that C–H bond cleavage involving the non-interacting H-atom occurs negligibly on the PdO(1 0 1) surface.

In our recent study of H_2 dissociation, we identified a facile dissociation pathway that involves rotation of the H_2 molecule lying parallel to the cus-Pd row to yield a final dissociated state where one of the H atoms is firmly bound on top of the cus-O site. We have generated a similar pathway for cleavage of a downward-oriented C–H bond of the adsorbed methane molecule. In this pathway (shown in Fig. 10b), the CH_4 molecule first undergoes a rotation and subsequent elongation of the C–H bond and then dissociates to a final state that is very similar to that found for the first pathway. However, this second pathway results in a much lower barrier of 64.2 kJ/mol, indicating that the η^2 interaction strongly facilitates C–H bond cleavage. The only difference between the final states in the two pathways is a small rotation of the methyl group, but the energies are nearly degenerate. We have confirmed that the final state(s) are indeed minima, but there are very low frequency (~50 cm^{-1}) rotational modes involving the methyl species. While the quantitative values of the barriers for methane activation determined with DFT should be taken with caution due to the lack of dispersion interactions, our results clearly show that dative bonding between the alkane molecule and the cus-Pd atom lowers the C–H bond cleavage barrier by more than 100 kJ/mol for CH_4. Future studies will incorporate DFT-D implementations to more accurately

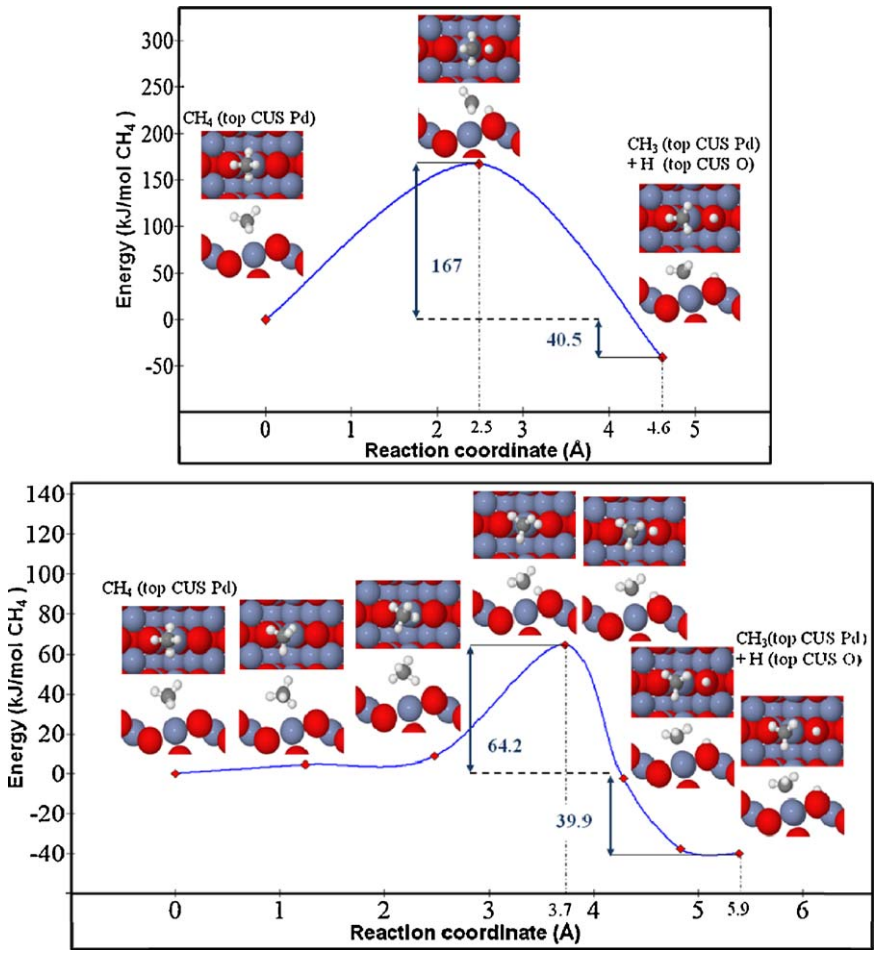

Fig. 10. The DFT-predicted pathway for initial C–H bond cleavage of methane on PdO(1 0 1) through (a) the non-interacting H atom and (b) the H atom involved in the four-center η^2 interaction with a cus-Pd atom.

predict both the adsorption and activation energies for methane and other alkanes on the PdO(1 0 1) surface. Once more accurate values incorporating dispersion are known, we can estimate the CH_4 dissociation rates at commercially relevant temperatures and pressures using transition state theory. Finally, the mode softening shows strong dependence for the η^1 interactions with primary versus secondary carbon groups on *n*-butane, so C–H activation studies of *n*-butane will be helpful in correlating mode softening to preferential C–H bond activation.

6. Summary

We investigated the molecular adsorption and dissociation of *n*-butane on a PdO(1 0 1) thin film using TPRS experiments and DFT calculations. The TPD results reveal that *n*-butane molecules populate a low-coverage state on PdO(1 0 1) that is more strongly bound than *n*-butane molecules physisorbed on Pd(1 1 1). This behavior is similar to that seen with smaller alkanes and arises from the formation of an *n*-butane σ-complex on PdO(1 0 1). The adsorption energy of the *n*-butane σ-complex continues a linear trend reported previously for the adsorption energy versus chain length relation of C_1 to C_3 *n*-alkane σ-complexes on PdO(1 0 1). This *E* versus *N* relationship demonstrates that dative bonding produces a similar enhancement in alkane binding on PdO(1 0 1) versus Pd(1 1 1) with increasing chain length up to *n*-butane. Our TPRS results also show that a fraction of the *n*-butane layer undergoes C–H bond cleavage on PdO(1 0 1) under the conditions investigated and that the resulting fragments are completely oxidized by the surface upon continued heating. The evolution of product yields with increasing *n*-butane coverage, as well as the results of site blocking experiments, provide strong evidence that the *n*-butane σ-complex acts as the precursor to initial C–H bond cleavage on PdO(1 0 1).

DFT calculations confirm that *n*-butane molecules bind relatively strongly on PdO(1 0 1) by forming σ-complexes on the cus-Pd rows. The calculations predict that the favored bonding geometry for *n*-butane is an η^1(2H) configuration in which the *n*-butane molecule lies parallel to the cus-Pd row and forms two H–Pd coordinate bonds. Our calculations reveal that steric repulsions between the terminal alkyl groups and the surface disrupt the bonding achieved in the η^2 configurations of *n*-butane, resulting in a strong preference for *n*-butane to adopt the η^1(2H) configuration along the cus-Pd row. In general, this steric effect causes the preferred bonding geometry of alkane σ-complexes on PdO(1 0 1) to change from η^2 to η^1 configurations with increasing chain length, with the η^1 configurations becoming preferred for molecules larger than propane.

The DFT calculations also demonstrate that the formation of alkane σ-complexes on PdO(1 0 1) weakens the coordinated C–H bonds, making them easier to cleave. We firstly predict that the coordinated C–H bonds elongate and undergo significant vibrational mode softening. The extent of C–H bond weakening caused by the dative interaction generally correlates with the stability of the alkyl radicals. Additionally, we find that coordination with the Pd center lowers the energy barrier for C–H bond cleavage by more than 100 kJ/mol for CH_4 adsorbed in the η^2 configuration. Given the more pronounced C–H bond weakening seen for the larger alkanes,

we anticipate that the dative bonding interaction will lower the C–H bond cleavage barriers for these molecules to an even greater extent than that predicted for methane. A key finding is that the formation of relatively strongly-bound σ-complexes on PdO(1 0 1) serves to electronically activate alkane C–H bonds in addition to prolonging the surface lifetimes of these reactive precursors. These results suggest the possibility that adsorbed σ-complexes play a general role as precursors for alkane activation on transition metal oxide surfaces.

Acknowledgements

We gratefully acknowledge financial support for this work provided by the Department of Energy, Office of Basic Energy Sciences, Catalysis Science Division through grant number DE-FG02-03ER15478. We also acknowledge the University of Florida High-Performance Computing Center (http://hpc.ufl.edu) for providing computational resources for performing some of the calculations reported in this paper.

References

[1] J.F. Weaver, A.F. Carlsson, R.J. Madix, Surf. Sci. Rep. 50 (2003) 107.
[2] R.B. Anderson, K.C. Stein, J.J. Feenan, L.J.E. Hofer, J. Ind. Eng. Chem. 53 (1961) 809.
[3] R.J. Farrauto, M.C. Hobson, T. Kennelly, E.M. Waterman, Appl. Catal. A 81 (1992) 227.
[4] R.J. Farrauto, J.K. Lampert, M.C. Hobson, E.M. Waterman, Appl. Catal. B 6 (1995) 263.
[5] R. Burch, F.J. Urbano, Appl. Catal. A 124 (1995) 121.
[6] R. Burch, F.J. Urbano, P.K. Loader, Appl. Catal. A 123 (1995) 173.
[7] J.G. McCarty, Catal. Today 26 (1995) 283.
[8] J.N. Carstens, S.C. Su, A.T. Bell, J. Catal. 176 (1998) 136.
[9] A.K. Datye, J. Bravo, T.R. Nelson, P. Atanasova, M. Lyubovsky, L. Pfefferle, Appl. Catal. A 198 (2000) 179.
[10] P. Salomonsson, S. Johansson, B. Kasemo, Catal. Lett. 33 (1995) 1.
[11] R.S. Monteiro, D. Zemlyanov, J.M. Storey, F.H. Ribeiro, J. Catal. 199 (2001) 291.
[12] H. Gabasch, K. Hayek, B. Kloetzer, W. Unterberger, E. Kleimenov, D. Teschner, S. Zafeiratos, M. Haevecker, A. Knop-Gericke, R. Schloegl, B. Aszalos-Kiss, D. Zemlyanov, J. Phys. Chem. C 111 (2007) 7957.
[13] C.F. Cullis, B.M. Willatt, J. Catal. 83 (1983) 267.
[14] P.D. Szuromi, J.R. Engstrom, W.H. Weinberg, J. Chem. Phys. 80 (1984) 508.
[15] C.B. Mullins, W.H. Weinberg, J. Chem. Phys. 92 (1990) 4508.
[16] S.A. Soulen, R.J. Madix, Surf. Sci. 323 (1995) 1.
[17] A.V. Hamza, H.P. Steinruck, R.J. Madix, J. Chem. Phys. 86 (1987) 6506.
[18] P.D. Szuromi, J.R. Engstrom, W.H. Weinberg, J. Phys. Chem. 89 (1985) 2497.
[19] D.F. Johnson, W.H. Weinberg, J. Chem. Phys. 101 (1994) 6289.
[20] J.F. Weaver, M.A. Krzyzowski, R.J. Madix, Surf. Sci. 393 (1997) 150.
[21] J.F. Weaver, S.P. Devarajan, C. Hakanoglu, J. Phys. Chem. C 113 (2009) 9773.
[22] J.F. Weaver, C. Hakanoglu, J.M. Hawkins, A. Asthagiri, J. Chem. Phys. 132 (2010) 024709.
[23] C. Hall, R.N. Perutz, Chem. Rev. 96 (1996) 3125.
[24] A.E. Shilov, G.B. Shul'pin, Chem. Rev. 97 (1997) 2879.
[25] J.A. Labinger, J.E. Bercaw, Nature 417 (2002) 507.
[26] C. Hakanoglu, J.M. Hawkins, A. Asthagiri, J.F. Weaver, J. Phys. Chem. C 114 (2010) 11485.
[27] A.L. Gerrard, J.-J. Chen, J.F. Weaver, J. Phys. Chem. B 109 (2005) 8017.
[28] H.H. Kan, R.B. Shumbera, J.F. Weaver, J. Chem. Phys. 126 (2007) 134704.
[29] H.H. Kan, R.B. Shumbera, J.F. Weaver, Surf. Sci. 602 (2008) 1337.
[30] H.H. Kan, J.F. Weaver, Surf. Sci. 602 (2008) L53.
[31] H.H. Kan, J.F. Weaver, Surf. Sci. 603 (2009) 2671.
[32] J.F. Weaver, M. Ikai, A. Carlsson, R.J. Madix, Surf. Sci. 470 (2001) 226.
[33] A.F. Carlsson, R.J. Madix, J. Phys. Chem. B 104 (2000) 12237.
[34] G. Kresse, J. Furthmuller, Comput. Mater. Sci. 6 (1996) 15.
[35] G. Kresse, J. Furthmuller, Phys. Rev. B 54 (1996) 11169.
[36] G. Kresse, J. Hafner, Phys. Rev. B 47 (1993) 558.
[37] G. Kresse, J. Hafner, Phys. Rev. B 49 (1994) 14251.
[38] H.H. Kan, R.C. Colmyer, A. Asthagiri, J.F. Weaver, J. Phys. Chem. C 113 (2009) 1495.
[39] G. Kresse, D. Joubert, Phys. Rev. B 59 (1999) 1758.
[40] P.E. Blochl, Phys. Rev. B 50 (1994) 17953.
[41] J.P. Perdew, K. Burke, M. Ernzerhof, Phys. Rev. Lett. 77 (1996) 3865.
[42] T. Pillo, R. Zimmerman, P. Steiner, S. Hufner, J. Phys.: Condens. Matter 9 (1997) 3987.
[43] M. Sierka, J. Sauer, J. Chem. Phys. 112 (2000) 6983.
[44] T. Kerber, M. Sierka, J. Sauer, J. Comput. Chem. 29 (2008) 2088.
[45] R.A. Olsen, G.J. Kroes, G. Henkelman, A. Arnaldsson, H. Jonsson, J. Chem. Phys. 121 (2004) 9776.
[46] G. Henkelman, H. Jonsson, J. Chem. Phys. 113 (2000) 9978.
[47] G. Henkelman, B.P. Uberuaga, H. Jonsson, J. Chem. Phys. 113 (2000) 9901.
[48] S.L. Tait, Z. Dohnalek, C.T. Campbell, B.D. Kay, J. Chem. Phys. 125 (2006) 234308.
[49] J.A. Hinojosa Jr., H.H. Kan, J.F. Weaver, J. Phys. Chem. C 112 (2008) 8324.
[50] K.A. Fosser, R.G. Nuzzo, P.S. Bagus, C. Woll, J. Chem. Phys. 118 (2003) 5115.